

FineServe: Precision-Aware KV Slab and Two-Level Scheduling for Heterogeneous Precision LLM Serving

Kyungmin Bin*, Seungbeom Choi*, Jimyoung Son, Jieun Choi, Daseul Bae, Daehyeon Baek,
Kihyo Moon, Minsung Jang, Hyojung Lee[†]
Cloud Research Team, Samsung SDS

Abstract

Recent advances in Post-Training Quantization (PTQ) techniques have significantly increased demand for serving quantized large language models (LLMs), enabling higher throughput and substantially reduced memory usage with minimal accuracy loss. Quantized models address memory constraints in LLMs and enhance GPU resource utilization through efficient GPU sharing. However, quantized models have smaller KV block sizes than non-quantized models, causing limited memory efficiency due to memory fragmentation. Also, distinct resource usage patterns between quantized and non-quantized models require efficient scheduling to maximize throughput. To address these challenges, we propose FineServe, an inference serving framework for mixed-precision LLMs. FineServe's key contributions include: (1) KV Slab, a precision-aware adaptive memory management technique dynamically allocating KV cache based on model quantization characteristics, significantly reducing GPU memory fragmentation, and (2) a two-level scheduling framework comprising a global scheduler that places models to GPUs based on request rates, latency SLOs, and memory constraints and efficiency, and a local scheduler that adaptively adjusts batch sizes according to real-time request fluctuations. Experimental results demonstrate that FineServe achieves up to 2.2× higher SLO attainment and 1.8× higher token generation throughput compared to the state-of-the-art GPU sharing systems.

1 Introduction

Large Language Models (LLMs) have rapidly been adopted in various applications, such as chatbots [2, 10, 21], automated code generation [16], and search engines [24], leading to substantial workload growth. The growing accuracy demands increase model size, push GPU memory to its limits, and make memory throughput a dominant bottleneck for inference [9]. Post-Training Quantization (PTQ) mitigates this pressure by lowering the precision of weights, activations, and the attention KV cache (e.g., FP8, INT8, INT4), which reduces memory footprint and often improves throughput with minimal accuracy loss. Mixed-precision deployments have therefore become more common, spanning from the original FP16 to FP8 variants [32], and much aggressive quantization schemes such as AWQ [14] and QoQ [15].

*The first two authors contribute equally and are listed alphabetically.

[†]Corresponding author (hyojung.lee.248@gmail.com).

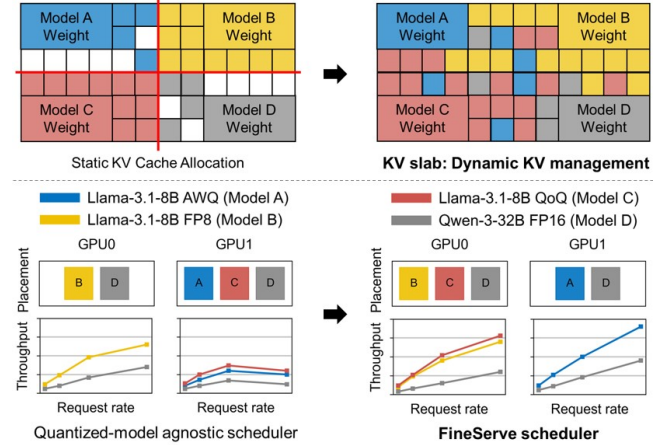


Figure 1. Main contributions of FineServe: KV slab for flexible and dynamic KV memory management (top) and quantized-model aware scheduling for efficient resource allocation (bottom). KV slab enables co-located models to share memory regardless of models' heterogeneous precisions. FineServe scheduler places models to the GPUs according to the precision of weights, activations, and KVs, thus it avoids contention and achieves higher throughput.

With the growing prevalence of quantized models, efficient management of GPU resources has become critical to address throughput and latency demands. Since quantized models require less memory, serving a single model on a GPU is not resource-efficient. A natural solution to increase resource efficiency is to share multiple models on a GPU.

However, serving mixed-precision models on shared GPUs raises two coupled challenges. First is KV memory management as shown in Figure 1. Serving frameworks such as vLLM [31] and SGLang [28] partition the KV cache statically per model, which strains capacity when co-located models have time-varying demand. A shared KV pool is an intuitive alternative because models borrow idle memory as workload fluctuates. However, heterogeneous token and KV block sizes due to different precisions and tensor parallelism create a dilemma when designing a shared KV pool. Using inconsistent block sizes causes external fragmentation. While using a single fixed block size eliminates external fragmentation, it incurs internal fragmentation for models with smaller token sizes, as many tokens must be packed into a single KV block compared to models that use larger token sizes. Thus, it requires a new KV cache management method for efficiently sharing GPU memory.

The second challenge is the GPU sharing policy. Models display different throughput for the same amount of incremented memory or computing resources, so equal shares or fixed ratios is inefficient. The scheduling policy should account for each model’s memory footprint (weights, activation buffers, and KV caches) and efficiently allocate GPU memory so that the memory per performance is maximized.

We present **FineServe**, a serving framework for mixed-precision LLMs that addresses both challenges:

- **KV Slab** is a precision-aware, adaptive KV cache manager. It pre-allocates a shared KV tensor per GPU. It carves it into uniform-sized slabs, which can be flexibly formatted to the KV block size of co-located LLM models, allowing heterogeneous KV blocks to be cached without memory fragmentation. This design enables each model to use a suitable KV block size for mitigating internal fragmentation, while a fixed slab size prevents external fragmentation. With our pre-allocation and view-based mapping design, current LLM frameworks seamlessly maintain logical KV cache block tables without modification of attention kernels. Furthermore, this design approach avoids frequent physical memory map-unmap driver calls, which have significant latency overheads [25].
- **Two-level scheduling** steers co-location and runtime batching. The global scheduler places models on GPUs regarding each model’s memory footprint (weights, activations and KV cache) and the remaining contested memory for KV cache. It ranks candidate placement using a memory-efficiency score, which is the expected number of tokens that increase per extra unit of residual KV memory. The local scheduler runs per node and enforces latency SLOs with adaptive batching. It predicts time-to-first-token (TTFT) for tentative batches and admits the largest SLO-safe batch.

Evaluation. We implement FineServe on top of the vLLM engine and evaluate it on a cluster of up to 16 NVIDIA H100 using the ShareGPT [29] dataset. Experiments cover a range of models and quantization variants. Results show that FineServe consistently improves both SLO attainment and throughput compared to state-of-the-art GPU sharing systems. In particular, at high request rates, FineServe sustains stable performance and achieves up to 2.2 \times higher SLO attainment and 1.8 \times higher token generation throughput.

2 Background

2.1 LLM Inference

LLM layers comprise linear layers and attention layers. Linear layers are often dominated by batched GEMM (General Matrix Multiplications) operations and are compute-intensive, with throughput driven by the GPU’s tensor-core performance. Attention layers operate in two phases: a prefill phase that processes the entire prompt and a decode phase that generates tokens sequentially. They maintain a KV cache that stores key-value pairs for all previously processed tokens at each layer.

For every new token, the model appends its keys and values and repeatedly reads the cache to compute attention. This high memory bandwidth usage makes attention memory-intensive and a frequent bottleneck in inference. This asymmetry motivates our focus on KV-cache-aware memory management and scheduling.

The amount of KV cache grows linearly with the number of processed tokens, so available KV memory bounds how many requests can run concurrently and how many additional tokens each request can generate. Because attention is memory-bound, the way KV memory is allocated and the precision of stored KV both directly impact throughput. We capture this characteristic and use it to determine how to share the GPU resource among multi-precision models, developed in Sections 5 and 6.

2.2 Post-Training Quantization (PTQ)

Post-Training Quantization (PTQ) converts a trained model to lower precision without additional training to reduce memory usage and computation. We treat the precisions of weights, activations, and the KV cache independently, and we use the notation $W\#A\#KV\#$. For example, W4A16 means INT4 weights with FP16 activations, and W8A8KV8 means FP8 weights, FP8 activations, and FP8 KV. If the KV part is omitted, we assume FP16-KV by default. The following quantization variants are supported in FineServe:

- **AWQ (W4A16)** [14] Activation-aware Weight Quantization lowers weights to 4 bits using activation statistics while keeping activations in FP16. This significantly lowers parameter memory and weight-bandwidth demand with minimal accuracy loss and executes on FP16 tensor cores.
- **FP8 (W8A8KV8)** [32]. Weights, activations, and KV are stored in FP8, leveraging FP8 tensor cores on Hopper-class GPUs to achieve higher arithmetic throughput compared to FP16 [31]. FP8 KV further reduces the size of the KV cache and lowers memory traffic during the decode phase.
- **QoQ (e.g., W4A8KV4)** [15]. Weights are INT4, activations are INT8, and KV is INT4, aiming to maximize memory savings. QoQ is the most aggressive quantization scheme in terms of reducing memory usage, pushing weights, activations, and KV to low precision. To mitigate the resulting accuracy loss, it employs several calibration strategies [15]. Consequently, under certain conditions, a throughput-accuracy tradeoff arises that limits achievable throughput, which we discuss in more detail in Section 3.1.

2.3 PagedAttention

PagedAttention [12] stores the KV cache in fixed-size blocks and uses a block table to present a logically contiguous tensor view. A sequence links as many blocks as it needs and grows by allocating new blocks, releasing blocks when they are no longer needed. Kernels read and write as if the KV were contiguous, while the physical blocks can be scattered in memory. This avoids large monolithic allocations and minimizes data

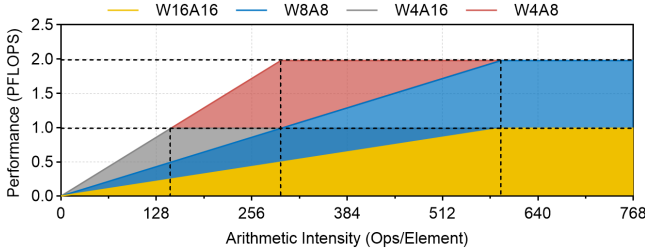


Figure 2. Roofline analysis of GEMM operations on multiple quantization variants. The baseline is the yellow region, FP16 (W16A16). The blue region shows the benefits of FP8 (W8A8) quantization over baseline, and the gray region shows such benefits from AWQ (W4A16) quantization over FP16. The red region shows additional benefits from QoQ (W4A8) over FP8 or AWQ quantization.

movement when sequence lengths change. PagedAttention is a core component of the current LLM serving frameworks, including VLLM and SGLang. In typical deployments, each model (served by its engine instance) maintains its own KV block pool and allocates blocks from that pool only. Models sharing a GPU thus do not directly borrow KV blocks from one another. Cross-model or cross-precision sharing, therefore, requires additional policies or a management layer on top of PagedAttention.

2.4 GPU Sharing

Sharing GPU resources in spatial [13], temporal [23], or using both [4, 6] has been shown to have potential for maximizing overall system throughput given limited GPU resources. Current sharing approach mainly focuses on compute sharing by using NVIDIA MPS [20] or NVIDIA MIG [20]. In contrast, memory management across co-located models remains under-explored, which may have substantial benefits in quantized LLM serving considering its reduced memory footprints, especially for KV cache. Each quantized KV cache shows different GPU memory efficiency as they yield different numbers of generated tokens given the same amount of GPU memory. Therefore, when mixed-precision LLMs are co-located in a single GPU, it is crucial to consider their precision to share GPU memory at runtime. Unfortunately, these characteristics of quantized LLMs in GPU sharing remain under-explored. We further discuss the characteristics of the quantized model serving in the following sections.

3 Motivation

3.1 Characteristics of Quantized Model Serving

(1) Computational characteristics. Quantized models exhibit distinct GPU resource usage patterns in LLM inference compared to non-quantized models because most operations are based on GEMM (General Matrix Multiplication), and changes in precision alter the tensor cores used to perform them. Figure 2 compares four quantization variants of the Llama3.1-8B model—FP16 (W16A16), FP8 (W8A8), AWQ (W4A16), and QoQ (W4A8)—showing that FP8 and QoQ

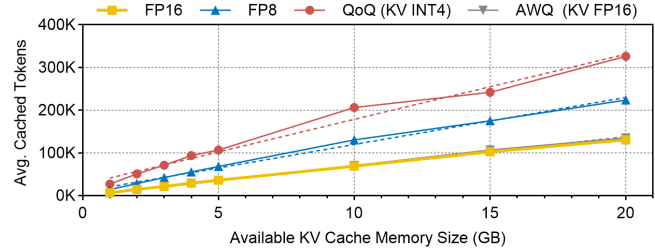


Figure 3. Average number of cached tokens during inference according to KV cache pool size. We use fixed input/output sequence length and request rate across models to show different marginal memory efficiency according to models’ token sizes. Lower KV cache precision models enable caching more tokens, given the available KV cache memory size.

models achieve twice the theoretical performance of FP16 and AWQ in compute-bound operations due to their use of FP8 tensor cores, while in memory-bound operations AWQ and QoQ perform best due to lower memory access and FP16 performs worst due to higher memory access. These characteristics directly influence inference behavior: the linear layers with large batched prompts and the attention layers’ prefill phases are typically compute-intensive, favoring FP8 models with higher compute throughput, whereas the decode phase is memory-bound, where lower-precision KV caches reduce memory traffic and improve performance. This diversity in roofline profiles explains the relative efficiency of quantized models and motivates the design of multi-LLM serving systems that allocate GPU resources more intelligently.

(2) Throughput according to the KV cache pool size. Figure 3 shows how the number of generated tokens depends on the KV cache pool size by plotting the average cached tokens for the same memory budget. We quantify this as *Marginal Memory Efficiency (MME)*, the additional tokens per unit of KV memory, defined as:

$$\mu_M(\mathcal{G}) = \frac{\Delta \text{generated tokens of model } M \text{ on } \mathcal{G}}{\Delta \text{KV memory}}$$

where M is a model placed on a GPU of TP-group \mathcal{G} . Intuitively, $\mu_M(\mathcal{G})$ is how many extra tokens M can produce when given a small increment of KV capacity on \mathcal{G} . In Figure 3, the slope corresponds to μ_M and is higher for lower KV-precision models (FP8 and QoQ). Because μ varies across models and precisions, how KV memory is allocated among co-located models has a crucial impact on end-to-end performance. Precision-aware KV memory management is therefore essential for maximizing throughput in multi-LLM serving, and FineServe uses μ in its model-to-GPU placement policy described in Section 6.2.

3.2 KV Cache Management for Quantized Models

(1) Limitations of static KV cache. When serving a single model on a single GPU, allocating a static KV cache pool in GPU memory and managing it with fixed-size pages (or

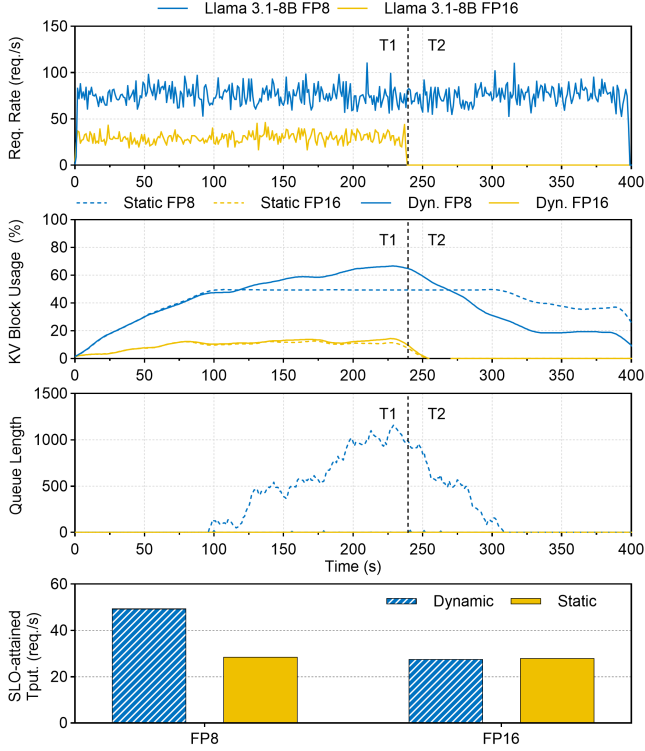


Figure 4. The KV block usage, queue length (the number of waiting requests), and SLO-attained throughput of the static and dynamic KV management for serving Llama 3.1-8B FP8 and Llama 3.1-8B FP16 models on a single GPU with ShareGPT dataset. We used *KV Slab* for dynamic KV management, which is discussed in Section 5. Statistically, reserving KV cache memory limits the flexible use of GPU cache memory, causing reduced SLO-attained throughput.

blocks) via a page table, as in paged attention [12], is a practical approach for KV cache management. However, when multiple LLMs are co-located and share GPU resources, static partitioning can reduce throughput and increase latency because each model is confined to a fixed, pre-allocated portion of memory. In contrast, a dynamic KV cache pool enables sharing the KV cache memory across the co-located models. Such a flexible GPU memory sharing approach adaptively utilizes GPU memory under dynamic real-world workload scenarios of serving multiple LLMs.

We compare the two approaches on ShareGPT using two co-located models on a single GPU: Llama 3.1-8B FP16 (model A) and its FP8-quantized variant W8A8KV8 (model B), under different request rate patterns. Figure 4 shows KV cache utilization, queue length (the number of waiting requests), and SLO-attained throughput for each model. In T1, both models run concurrently with different average request rates, but under static partitioning, model B cannot use model A's reserved memory even when A is idle. This limitation continues in T2, model A's KV memory, which is still statically allocated and is blocked from use by model B, leaving that portion of memory unused. This memory wall increases B's

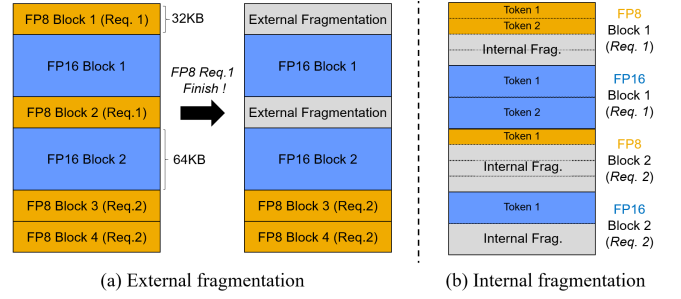


Figure 5. Illustrations of external and internal memory fragmentation with dynamically sharing GPU memory.

queue and reduces SLO-attained throughput. In contrast, the dynamic approach flexibly utilizes the KV memory without such a memory wall, keeps the queue short, resulting in higher SLO-attained throughput. This highlights that dynamic KV cache memory management is crucial for serving multiple LLMs that share GPU memory.

(2) Challenges of dynamic KV cache management. While a dynamic KV cache memory management approach enables efficient sharing of GPU memory across co-located models, it introduces three challenges when quantized models are involved, stemming from heterogeneous token sizes and context switching overhead from frequent memory allocation and deallocation.

C1. External fragmentation by the different KV block sizes: The heterogeneous KV block sizes cause external fragmentation in memory. The KV block size is defined as the quantization parameters (Quant.Params) plus the product of the number of tokens per block (TokensPerBlock) and the number of bytes required for each token (TokenSize):

$$\text{KVblocksize} = \text{TokensPerBlock} \times \text{TokenSize} + \text{Quant.Params}.$$

The token size of a model varies for TP degree and KV precision, following:

$$\text{TokenSize} = \frac{\#\text{Heads}}{\text{TP degree}} \times \text{HeadDim} \times 2 \times \text{bytes(precision)},$$

where the *bytes* vary according to the model's precision, e.g., FP16 is 2 bytes and INT4 is 0.5 bytes. Furthermore, KV-quantized models (e.g., QoQ [15]) store per-token quantization parameters such as scaling factors in each KV block for online dequantization, making block sizes more heterogeneous and challenging to manage KV cache memory without fragmentation. Such parameters make the KV block size more heterogeneous, making it challenging to manage the KV cache memory without fragmentation. Heterogeneous KV block size causes significant *external fragmentation* between co-located models, leading to decreased throughput of the overall system. Figure 5(a) shows an example in which external fragmentation occurs after the first request of the FP8-quantized model has been freed.

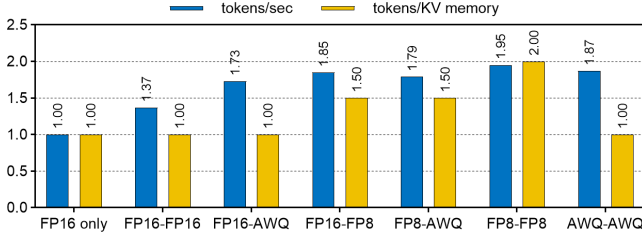


Figure 6. Impact of GPU sharing. Normalized throughput (blue bar) and normalized generated tokens per unit KV cache memory (yellow bar). The baseline is single model placement (FP16 only).

C2. Internal fragmentation from heterogeneous token sizes: Using a fixed size of KV cache block across the co-located models can mitigate external memory fragmentation. Unfortunately, this approach deteriorates *internal fragmentation* for models with smaller token sizes, because many tokens must be packed into a single KV block. For example, in Figure 5, the half token size of the FP8-quantized model incurs internal fragmentation inside its blocks. Since most serving systems do not support cross-request block sharing, such internal fragmentation increases in proportion to the number of requests for that model.

C3. Context switching overhead: To support cross-model KV cache memory sharing, a recent study [37] adopts CUDA Virtual Memory Management (VMM) driver APIs [19]. VMM allows on-demand memory allocation while maintaining contiguous KV cache memory spaces of existing LLM engines. With this approach, the engine reserves KV cache memory as virtual memory addresses and maps them to physical memory addresses on demand during inference. However, this mapping requires VMM driver calls that cause context switch overheads [25] on the order of tens of microseconds per call. Growing a KV block of a request adds per-layer driver calls, resulting in several milliseconds of latency. Such latency overhead grows proportionally to the number of requests during multi-LLM serving, degrading SLO attainment of the system.

These challenges directly limit the efficiency of a shared KV tensor in mixed-precision multi-LLM serving. Motivated by these issues, we design and implement **KV slab** (detailed in Section 5), a memory management scheme inspired by the slab allocator in operating systems.

3.3 Impacts of GPU Sharing: Throughput and Memory Efficiency

GPU sharing can improve throughput and memory efficiency by allowing models to share compute and memory resources, thereby making better use of idle capacity. The following presents the increases in aggregated throughput and KV memory efficiency that arise when quantized models share a GPU.

Normalized aggregated throughput. Figure 6 (blue bars) reports the aggregated throughput of two co-located models normalized to the FP16-only baseline. We evaluate six pairs, FP16-FP16, FP16-AWQ, FP16-FP8, FP8-FP8, FP8-AWQ,

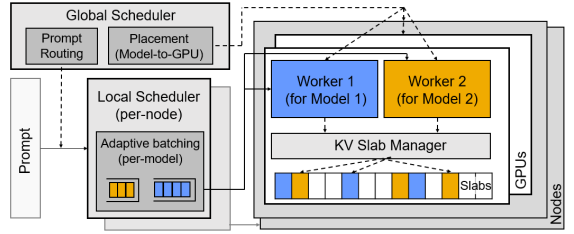


Figure 7. Overall Architecture of FineServe.

AWQ-AWQ, using NVIDIA MPS to serve two models concurrently. In all cases, the aggregated throughput exceeds the FP16-only baseline. The improvement is not a perfect 2× due to sharded SM and bandwidth contention, but GPU sharing with quantized models shows a high throughput achievement. Especially, FP8-FP8 achieves 1.95×, which is close to the ideal with negligible loss. This confirms that co-location can translate quantization benefits into higher end-to-end throughput under the same device resource.

Tokens per unit memory for KV cache. We quantify memory efficiency with tokens per unit of KV memory, i.e., marginal memory efficiency, under co-located models. Figure 6 (yellow bars) shows that, relative to the FP16-only baseline, any pair that includes an FP8-quantized model (KV8) increases the average tokens-per-memory because lower precision KV stores more tokens in the same memory resource. This characteristic motivates a precision-aware placement policy, discussed in Section 6.2.

4 Overall Architecture of FineServe

FineServe introduces two ideas: a precision-aware KV manager that shares a pre-allocated KV tensor across co-located models, and a two-level scheduler that meets per-request latency SLOs while allocating memory by marginal memory efficiency. As illustrated in Figure 7, FineServe consists of vLLM-based workers, a per-GPU KV slab manager, a global scheduler, and per-node local schedulers. Each worker is bound to a specific model and a specific GPU and runs independently. The main components of FineServe are as follows:

Workers. Run on top of the vLLM engine. A worker is created per (model shard × GPU). If TP is N , the model runs with N workers spread across N GPUs. If data parallelism (DP) creates replicas of the same model, each replica is treated as a separate model for placement and scheduling and owns its own set of workers. Multiple workers can run on the same GPU when different models are co-located.

KV slab manager. Resides on each GPU. Manages the shared KV tensor and divides it into slabs of uniform physical size. Workers request and release blocks to KV slab manager by specifying their KV block size.

Global scheduler. Uses profiling to capture per-model characteristics such as latency and average memory footprints.

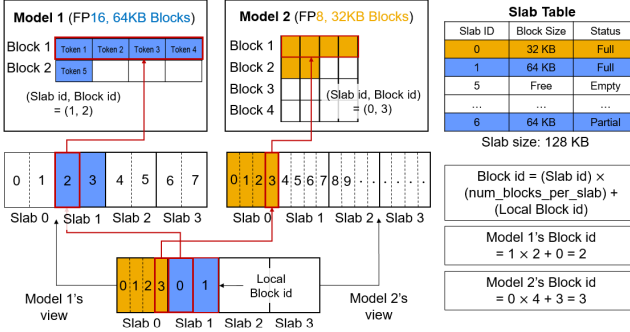


Figure 8. Model 1 and 2 have different views of physical GPU memory. The slab manager assigns local block 0 of slab 1 to Model 1 and local block 3 of slab 0 to Model 2. Each model computes its own block ID. Model 1 has $(\text{slab id}, \text{blk id}) = (1, 2)$ and Model 2 has $(0, 3)$. The slab table records the status of slab allocation.

Decides model-to-GPU placement and computes target request rates for the local schedulers across nodes.

Local scheduler. Runs on each node. Maintains per-model queues and adjusts batch size online using latency predictions so that per-request SLOs are met.

5 KV Slab: Dynamic KV Cache Management

KV slab, inspired by the slab allocator [3] in operating systems, is a core component of FineServe for mixed-precision multi-LLM serving. The slab allocation approach is designed to avoid memory fragmentation caused by heterogeneous object sizes by caching objects in a fixed-sized memory chunk, which is called a *slab*. Motivated by this, we design a *KV slab* that manages shared KV cache memory with a fixed size of memory chunk that can be flexibly formatted to the KV block size of co-located LLM models, allowing heterogeneous KV blocks to be cached without memory fragmentation. The detailed structure of the KV slab is illustrated in Figure 8. Our KV slab design addresses three issues discussed earlier in Section 3.2: (C1) external fragmentation when multiple KV block sizes co-exist, (C2) internal fragmentation from heterogeneous TokenSize, and (C3) mapping overhead from frequent memory driver calls.

5.1 Rationale of KV Slab

Avoiding memory fragmentation. The key idea of KV slab is to manage the shared KV cache memory with a fixed size of memory chunk, called a *KV slab*, which can contain multiple KV blocks given a block size. The block size determines the number of KV blocks in a KV slab. This design avoids external fragmentation (C1 in Section 3.2) while maintaining a suitable KV block size for each quantized LLM, mitigating internal fragmentation (C2 in Section 3.2).

Avoiding runtime memory allocation and free overheads. Our KV slab design also addresses the context switching overhead challenge (C3 in Section 3.2), by pre-allocating a single large shared KV tensor and using view-based mapping

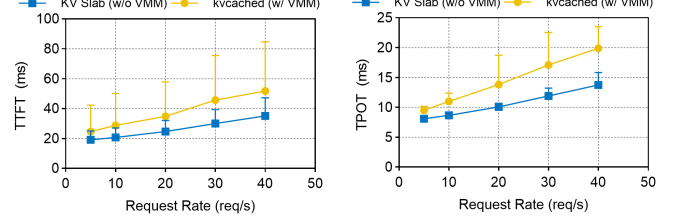


Figure 9. Measured TTFT and TPOT of KV slab and the kvcached library [37], which uses CUDA VMM, when serving Llama 3.1-8B FP16 on ShareGPT workload datasets. CUDA VMM introduces memory allocation and free overheads, which significantly degrade TTFT and TPOT performance as the request rate increases. This highlights that the context switching overhead is non-negligible and can lead to substantial SLO violations in practice.

in LLM engines. As shown in Figure 8, a fixed-size KV slab can be viewed as a different number of blocks depending on block size, without invoking any memory-related driver calls at runtime. With this design, the only requirement is to precisely map the physical shared KV memory address to the logical block IDs of co-located LLM engines. This allows each LLM engine to maintain its own logical KV block table and execute the existing attention kernel without modification.

Figure 9 shows the measured time-to-first-token (TTFT) and time-per-output-token (TPOT) performance of KV slab and kvcached [37], which uses CUDA VMM driver APIs for dynamic KV cache management, for serving Llama 3.1-8B FP16 on ShareGPT workload datasets. kvcached shows higher TTFT and TPOT than KV slab, and the performance gap widens as request rate increases. This highlights that frequent memory-relevant driver calls are non-negligible and can cause significant SLO violations in practice.

5.2 KV Slab Manager

Shared KV tensor coordination. The key role of the KV slab manager is to coordinate the physical shared KV tensor across co-located LLM engines without causing memory corruption at runtime. This coordination is achieved by precisely mapping physical memory addresses to each engine’s logical block ids. The KV slab manager manages the shared KV tensor by mapping the slab ID and local block ID with a slab to each LLM engine’s block ID. Figure 8 explains an example of block allocation and block numbering. Each engine’s block ID is calculated as follows:

$$\text{Blk ID} = (\text{slab ID}) \times (\# \text{ of blks per slab}) + (\text{local blk ID}).$$

Block allocation and release flow. The KV slab manager creates, allocates, and frees slabs in the shared KV tensor and keeps their metadata in a *KV slab table*, as shown in Figure 8. On each GPU, all slabs have the same size, chosen as a multiple of the least common multiple of the co-located model’s KV block sizes. The manager finds a slab with the key or carves a new one, allocates a block, and returns a (slab ID, block ID) pair. Each slab is keyed by its KV block

size and stores blocks only of that size. Different slabs can use different keys. Given the requested slab key (KV block size), the manager looks up the matching pool, allocates a free block from a matching slab (or creates a new slab), updates the slab’s state, and returns the (slab id, block id) to the engine. When a block is released, the manager clears the corresponding entry and updates the slab’s state. If a slab becomes empty, the manager returns its memory to the shared KV tensor as free space. A new slab will be carved from the shared KV tensor on demand. The slab table records slab state (FREE, PARTIAL, FULL) and the mapping from blocks to slabs. This flexible slab pool design naturally determines the slab pool size (i.e., how many slabs are formatted into each block size) at runtime, effectively coordinating shared KV memory resources across co-located LLM models.

6 Two-level Scheduler

FineServe uses a two-level scheduler. The global scheduler places models on GPUs based on profiled latency, memory footprints (weights, profiled activations, and profiled KV cache), marginal memory efficiency, and SLO feasibility. The local scheduler runs on each node and, by predicting completion latency in real time, chooses per-model batch sizes online that keep the SLO latency.

6.1 Scheduling Principles and Objectives

Our goal is to maximize total throughput subject to per-request latency SLOs while using GPU memory efficiently. We use marginal memory efficiency (MME, μ) as the central signal. For a model M placed on GPU (or TP-group) \mathcal{G} , recall the definition of $\mu_M(\mathcal{G})$ is:

$$\mu_M(\mathcal{G}) = \frac{\Delta \text{generated tokens of model } M \text{ on } \mathcal{G}}{\Delta \text{KV memory}}.$$

We partition memory into *fixed* and *contested* parts. For each model, a base footprint, consisting of weights and profiled averages for activation memory and KV cache, is treated as a fixed cost charged to any GPU that hosts that model’s shard. Only the remaining capacity on that GPU is considered *contested memory*. At placement time, we evaluate candidate GPUs using a score that estimates the throughput lift from this contested memory. The exact formulation and the proxy we use appear in Section 6.2.

SLO feasibility is enforced at two levels. Offline, the global scheduler verifies that each placed model has at least one profiled operating point on its assigned GPU(s), a specific batch size, at which the predicted TTFT is within the SLO. Online, the local scheduler enforces the TTFT SLO using earliest-deadline-first (EDF) and a chunked prefill latency model, admits the largest batch whose prefill finishes before the earliest deadline. Note that, without loss of generality, we use per-model SLOs rather than per-request SLOs, under the assumption that the requests from the same model exhibit similar usage patterns.

Algorithm 1: Model-to-GPU Placement

Input: LLM list \mathcal{M} , GPU cluster C , Total memory $T_{\mathcal{G}}$ of GPU \mathcal{G} , Estimated required memory F_M of model $M \in \mathcal{M}$

Output: Placement list \mathcal{P}

- 1 Sort models by F_M in descending order
- 2 $\mathcal{P} \leftarrow []$
- 3 **for** $M \in \mathcal{M}$ **do**
- 4 **for** $\mathcal{G} \in C$ **do**
- 5 $K_{\text{rem}}(\mathcal{G}) \leftarrow T_{\mathcal{G}} - \sum_{m \in \mathcal{G}} F_m$
- 6 update score($\mathcal{G}|M$)
- 7 $\mathcal{G}_M \leftarrow \arg \max_{\mathcal{G}} \text{score}(\mathcal{G}|M)$
- 8 $\mathcal{P} \leftarrow \text{append}(\mathcal{P}, \mathcal{G}_M)$
- 9 **return** \mathcal{P}

FineServe’s algorithms use TTFT SLO as the latency constraint rather than the end-to-end latency SLO, which consists of both TTFT and TPOT. TPOT grows with the output length and is difficult to predict before inference completes. In contrast, TTFT can be expected at dispatch time, since it is affected by queueing delay and prefill latency, which are in turn determined by the request’s arrival time and prompt length. In addition, by considering the TTFT SLO, requests that would otherwise violate the end-to-end latency SLO due to queueing delay can be proactively filtered. TTFT-aware scheduling also enables placement strategies that allocate sufficient compute resources to each model in order to satisfy the latency of the compute-intensive prefill phase. FineServe’s algorithms, in tandem with fixed and contested part memory allocation, ensure balanced provisioning of GPU compute and memory resources across co-located models.

6.2 Global Scheduler: Model-to-GPU

The global scheduler chooses a model-to-GPU placement that maximizes total throughput while meeting latency SLOs and GPU memory budgets. As described in Algorithm 1, inputs are the model set \mathcal{M} , the placement candidates in cluster C (a single GPU if $TP = 1$, or a TP -sized GPU group if $TP > 1$), each candidate’s memory budget $T_{\mathcal{G}}$ and base footprint F_M of model M (weights plus profiled average activations and KVs). F_M is measured at the smallest batch size whose profiled throughput meets M ’s expected request rate. If that batch size would violate the TTFT SLO, we meet the rate by increasing the number of data-parallel replicas ($DP > 1$) instead. DP replicas are treated as independent model instances.

Scoring GPUs. When evaluating where to place a model, we compute the *score* of each candidate GPU after charging base footprints. The rigorous score estimates the additional throughput obtainable by distributing the remaining contested

memory among all co-located models:

$$\text{score}(\mathcal{G}|M) \triangleq \max_{\Delta K_m > 0} \sum_{m \in \mathcal{G}'} \mu_m(\mathcal{G}') \cdot \Delta K_m, \quad (1)$$

$$\text{s.t. } \sum_{m \in \mathcal{G}'} \Delta K_m \leq K_{\text{rem}}(\mathcal{G}'), \quad (2)$$

where \mathcal{G}' denotes GPU \mathcal{G} after accommodating model M . Each model placed on \mathcal{G}' is denoted by $m \in \mathcal{G}'$. $K_{\text{rem}}(\mathcal{G}')$ is the remaining contested memory after charging base footprints, and the additional KV memory allocated to model m from the contested memory is ΔK_m . However, ΔK_m is difficult to estimate in practice. Thus, we use an acceptable approximation:

$$\text{score}(\mathcal{G}|M) \approx \frac{1}{|\mathcal{G}'|} \cdot \sum_{m \in \mathcal{G}'} \mu_m(\mathcal{G}') \cdot K_{\text{rem}}(\mathcal{G}'), \quad (3)$$

where $|\mathcal{G}'|$ is the number of models in \mathcal{G}' . The proxy has three desirable properties: (i) it reflects how much adding model M raises the group's average μ , (ii) for the same μ_M , smaller candidate groups $|\mathcal{G}'|$ see a larger increase in the average, so GPUs with fewer resident models are naturally favored, and (iii) huge μ_M values are tempered by the averaging, which prevents excessive bias toward a single model. This favors models that use extra KV well while not excluding higher-precision models with larger average footprints.

Algorithm 1: Placement. The global scheduler performs placement in two phases under a model-centric view. In the first phase, all models are sorted in descending order of their base footprint F_M , so that models with the most significant fixed memory costs are placed first. In the second phase, each model is considered in this order and evaluated across all candidate GPUs or TP-sized groups \mathcal{G} . For each candidate, the scheduler computes $\text{score}(\mathcal{G}|M)$, which estimates the benefit of placing model M on \mathcal{G} . The model is then assigned to the candidate GPU (or group) with the highest score. The resident set of that GPU is updated accordingly.

6.3 Local Scheduler: Adaptive Batching

The local scheduler runs on each node and enforces the TTFT SLO for every model while making efficient use of available GPU memory and compute resources. It maintains a separate queue for each model. Inputs include the set of waiting requests, the current time, and per-model hard caps on concurrent requests (N_{max}) and batched prompt tokens (T_{max}), both derived from the current remaining capacity in compute and memory.

Design rationale. Our algorithm fundamentally builds on the Moore-Hodgson algorithm [17] to meet the SLO, but adapts it to fit chunked prefill settings. The Moore-Hodgson algorithm is specialized for serving requests individually. As a result, the request sequence it produces is optimal only when the batch size is one. In this case, however, chunked prefill cannot be exploited, leading to performance degradation. When the sequence is executed with a batch size greater than one, the

Algorithm 2: SLO-aware Adaptive Batching

Input: LLM model M , max number of requests N_{max} of M , max number of batched tokens T_{max} of M , TTFT SLO slo_M of M , chunked prefill latency $TTFT(R)$ for a set of requests R , current waiting requests W , current time t .

Output: Set of requests S to be served.

```

1  $S \leftarrow \emptyset$ 
2  $D \leftarrow \emptyset$ 
3 for  $r \in W$  do
4    $d_r \leftarrow \text{arrival\_time}(r) + slo_M$ 
5   if  $t + TTFT(r) < d_r$  then
6      $S \leftarrow \text{add}(S, r)$ 
7   else  $D \leftarrow \text{add}(D, r)$ 
8  $W \leftarrow \text{remove}(W, D)$ 
9 Sort  $S$  by  $d_r$  in ascending order.
10 while true do
11    $r_0 \leftarrow \text{front}(S)$ 
12   if  $t + TTFT(S) < d_{r_0}$  then
13      $\text{break}$ 
14    $r_1 \leftarrow \text{longest\_request}(S)$ 
15    $S \leftarrow \text{remove}(S, r_1)$ 
16  $S \leftarrow \text{trim}(S, N_{\text{max}}, T_{\text{max}})$ 
17  $W \leftarrow \text{remove}(W, S)$ 
18 return  $S$ 

```

algorithm becomes theoretically sub-optimal. The reason is as follows: The algorithm tends to form larger batches of requests because it considers the processing time of each individual request, which is shorter than that of the entire batch. This leads to the conclusion that more requests will meet their deadlines. However, with chunked prefill, the processing time increases with the entire batch, which in turn increases the likelihood of SLO violations for requests with earlier deadlines. To address this issue, we modified the algorithm itself so that it forms a batch of requests to be served while explicitly ensuring that the SLO of the earliest-deadline request within the batch remains unviolated when the entire batch is processed by chunked prefill.

Algorithm 2: SLO-aware adaptive batching. The local scheduler processes waiting requests of a model by setting each request's deadline as its arrival time plus the model's SLO (line 4). Requests that cannot meet their deadline, even if processed individually and immediately, are dropped at once (lines 7-8). By dropping these requests, GPU memory and compute resources of the system become more available, thereby enhancing the likelihood of meeting the deadlines for other requests. The remaining requests are sorted in ascending order by their deadlines, following the EDF policy, and form a tentative batch S of requests to be served (lines 5-6, 9). The request with the earliest deadline acts as the anchor for the tentative batch of requests (line 11). The longest-running request is removed from the tentative batch as long as the

Table 1. Evaluated System Specification.

Component	Description
CPU	32× vCPU Intel Xeon Platinum 8468 @ 2.1 GHz, Hyper-threading enabled
GPU	4× NVIDIA H100 80GB SXM5 (700W)
GPU P2P	900 GB/s NVSwitch
PCIe	PCIe Gen5 $\times 16$
Memory	DDR5 720 GB allocated

Table 2. System Specification of AWS Nodes.

Component	Description
Instance	AWS p5.48xlarge $\times 2$
CPU	384 vCPUs per instance
GPU	8× NVIDIA H100 80GB per instance
Memory	2 TB per instance
Network	3200 Gbps with AWS Elastic Fabric Adapter
GPU P2P	900 GB/s NVSwitch

predicted prefill finish time of the batch exceeds the anchor’s deadline (lines 12-15).

To fully leverage chunked prefill, we focus on the prefill finish time of the entire batch of requests rather than individual requests, and this adjustment frees capacity to rebuild a new tentative batch, guaranteeing that admitted requests can be served within their SLOs. Finally, from the tentative batch, the batch of requests to be served is formed, ensuring that it adheres to the system constraints by not exceeding the maximum number of concurrent requests (N_{\max}) and the maximum number of batched tokens (T_{\max}) (line 16). In 7.3, we explain the effectiveness of our algorithm.

7 Evaluation

We evaluate FineServe to demonstrate its effectiveness in improving latency SLO attainment, throughput, and memory efficiency when serving mixed-precision LLMs. Experiments are conducted on various scales of GPU clusters using real-world traces and widely adopted quantized model variants. We compare against state-of-the-art baselines and analyze the contributions of each component.

7.1 Experimental Setup

We evaluate a prototype implementation of FineServe. For single-node experiments, the system is deployed on a multi-GPU server (Table 1), and for large-scale evaluation, we use two AWS EC2 p5.48xlarge instances (Table 2).

Baselines. We compare FineServe against two baselines:

- **Static^{*}:** GPU memory is statically partitioned per model, proportional to its required footprint (weights, activations, KV cache). Placement follows the same policy as FineServe, but prompts are scheduled with first-come-first-serve (FCFS) batching and without deadline guarantees.

Table 3. Evaluation Models and Their Quantization Variants.

Model	Quantization Variants
Llama3.1-8B	FP16, FP8 (W8A8KV8), AWQ (W4A16)
Llama3-8B	QoQ (W4A8KV4)
Llama3.1-70B	FP16, FP8 (W8A8KV8), AWQ (W4A16)
Qwen3-32B	FP16, FP8 (W8A8KV8)

- **Prism^{*}:** We compare the scheduling algorithms introduced in Prism [37]. Prism proposed a model-to-GPU heuristic placement that aims to balance the ratio of remaining KV cache usage to SLO-weighted request rates and a deadline-based prompt scheduling. We implemented the algorithms into FineServe and to provide a fair comparison, the baseline uses KV slab rather than kvcached [37] to allocate GPU memory across co-located models. This is because kvcached has non-negligible map/unmap overheads for CUDA VMM API call, as described in Figure 9.

Workloads. We use prompts sampled from the ShareGPT dataset. Since ShareGPT does not contain quantized models, we evaluate the quantized variants listed in Table 3. To create large input scenarios, we scale the request rate derived from ShareGPU by a fixed factor (e.g., 2 \times or 4 \times), which proportionally increases the load while preserving the request distribution. We sample random inter-arrival times from a Poisson random distribution, based on previous research [39] claiming real-world requests follow a Poisson distribution.

Models. As summarized in Table 3, the evaluation covers Llama 3.1-8B, Llama 3.1-70B, Llama 3-8B, and Qwen 3-32B [35]. Quantization variants include FP16, FP8 (W8A8KV8), AWQ (W4A16), and QoQ (W4A8KV4). We applied QoQ only to the Llama3-8B model, as it did not apply to the others.

Metrics. We report three primary metrics. First, TTFT SLO attainment is the fraction of requests whose TTFT meets the per-model latency SLO. The SLO is defined as the P95 prefill latency from the ShareGPT dataset. We also use a scaled SLO, which allows us to evaluate the system under varying latency targets. Second, throughput (req/s) is the number of requests completed per second. Third, token generation throughput (tokens/s) is the average number of output tokens generated per second during the decode phase, excluding prefill.

7.2 End-to-End Performance

We first evaluate the end-to-end performance on SLO attainment and token generation throughput under varying SLO scales and request rate scales. As shown in Figure 10, FineServe delivers the highest SLO attainment and the token throughput across both SLO scale and request rate scale experiments. With tighter SLOs, FineServe sustains high SLO attainment while Prism^{*} drops sharply and Static^{*} remains lower in tokens/s. As the request rate increases from 2 \times to 8 \times , FineServe keeps SLO attainment high and scales token throughput to about 2.3K tokens/s at 8 \times , whereas Prism^{*}

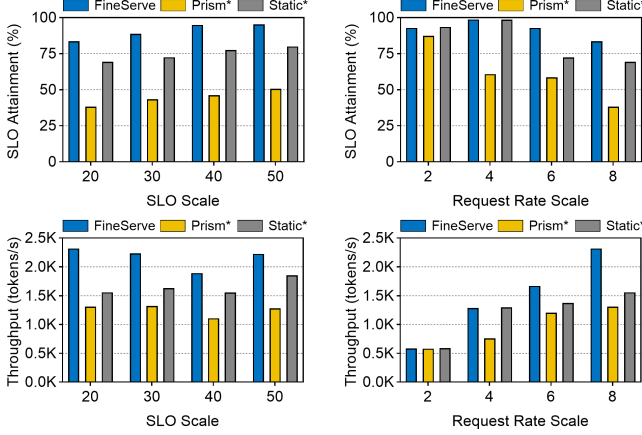


Figure 10. End-to-end performance comparison on SLO attainment and token generation throughput under varying SLO scales (with fixed rate scale 8) and request rate scales (with fixed SLO scale 20).

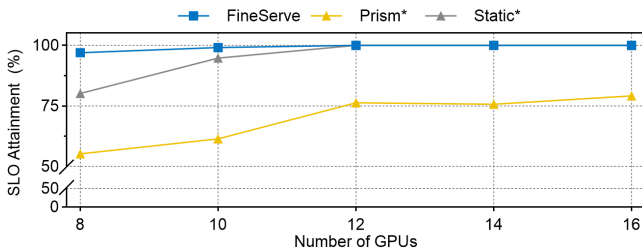


Figure 11. SLO attainments on multiple nodes.

saturates early and Static* grows slowly. These differences are also evident in the numbers. At SLO scale 20 and request scale 8, FineServe achieves 2.2 \times higher SLO attainment than Prism* and 1.2 \times higher than Static*, while in token generation throughput, it delivers 1.8 \times higher than Prism* and 1.5 \times higher than Static*.

These gains come from precision-aware placement and batch-aware local scheduling. FineServe’s global scheduler first charges each model’s base footprint (weights, profiled average activations, and KV), then assigns the remaining KV capacity to models with higher marginal memory efficiency (μ in Section 6), so residual memory goes where it produces the most tokens under the SLO. At runtime, FineServe combines the earliest-deadline-first strategy with chunked-prefill, batch-aware scheduling that preserves TTFT SLO while maximizing batch size. Prism* instead uses a quantization-agnostic heuristic that splits remaining KV by an SLO-to-request-rate ratio, and its local scheduler does not account for batching, so it underutilizes chunked prefill under load. Static* avoids contention with fixed partitions, but strands KV capacity when demand is imbalanced, which limits throughput.

Large-scale evaluation. We also evaluate how well FineServe can scale out with a larger number of GPUs residing on multiple nodes. Figure 11 reports the SLO attainment of each baseline when serving the same subset of models and rates.

Table 4. Placement Results (Placement Order) of Figure 12

Method	GPU 0		GPU 1	
	Model C (1st)	Model B (2nd), Model A (3rd)	Model A (2nd), Model B (3rd)	Model A (2nd)
FineServe				
Prism*				

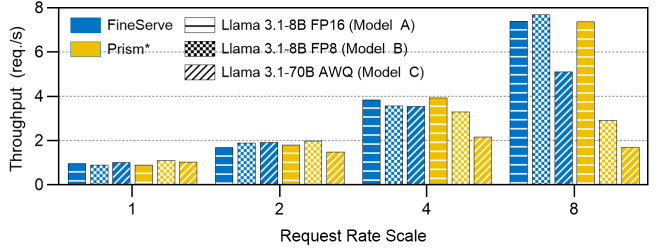


Figure 12. Impact of global scheduler: throughput comparison of FineServe and Prism* under scaled request rates.

We increase the number of GPUs from 8 to 16, adding two GPUs for each experiment. FineServe maintains a steady SLO attainment, where the minimum value is 96.9%, and Static* steadily increases from 80.1% as more GPUs are available, outperforming the results of Prism*. This is mainly due to the decreased SLO attainment of models that are co-located with AWQ (W4A16KV16) quantized models, where bit-precision agnostic placement, such as Prism*, tends to underestimate the memory usage.

The reported SLO attainment results of FineServe hint at cost savings of GPUs. By efficiently utilizing GPU memory, FineServe would be able to virtually offer cost savings for LLM service providers deploying quantized models. For instance, Prism* cannot achieve the same rate of SLO attainment of FineServe even with twice as many GPUs. In other words, FineServe can potentially reduce the required number of GPUs to at least half of the original number.

7.3 Ablation Study: Two-level Scheduler

Global scheduler evaluation. Figure 12 compares the global scheduler of FineServe against Prism* in terms of throughput (req/s) as the scaled request rate increases from 1 \times to 8 \times . For a fair comparison, cases are configured with a static KV partition and an FCFS local scheduler.

The placement results are summarized in Table 4. After placing two higher-priority models on separate GPUs, FineServe co-locates the third model (Model B, Llama3.1-8B FP8) with Model A (Llama3.1-8B FP16) on GPU1, while Prism* co-locates the third model (Model C, Llama3.1-70B AWQ) with Model B on GPU0. Under Prism*, the model placed alone (Model A) scales its throughput proportionally to the request rate, but the co-located models (B and C) suffer throughput degradation in the 4 \times -8 \times rate range. In contrast, FineServe sustains stable performance across all models and achieves up to 3 \times higher aggregated throughput than Prism* at 8 \times scaled rate.

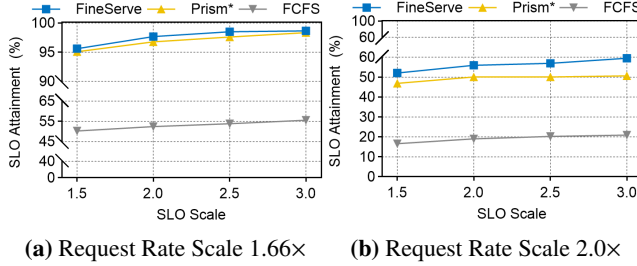


Figure 13. Impact of local scheduler: SLO attainment comparison of FineServe, Prism*, and FCFS under scaled SLOs.

The two key reasons FineServe maintains stable throughput even under high rates are (i) its placement order, determined by each model’s total resource demand (F_M in Section 6.2, and (ii) its scoring policy, which reflects marginal memory efficiency (μ). In contrast, Prism* orders placement by SLO-weighted request rate, which can push memory-intensive models to later positions. In such cases, preempted resources lower memory efficiency and reduce total throughput.

Local scheduler evaluation. To isolate the effect of the local scheduler, we evaluate scenarios where a single model is placed on a GPU and the KV cache is managed statically. We compare three schedulers: FineServe, Prism*, and FCFS. The experiment uses the Llama-3.1 8B FP16 model under two request rate scales: 1.66 \times in Figure 13a and 2.0 \times in Figure 13b. For each case, we set the SLO latency baseline to the P90 TTFT latency achieved by FCFS. Results show that FineServe achieves up to 45.34% higher SLO attainment than FCFS and up to 8.87% higher than Prism*. Both FineServe and Prism* outperform FCFS due to their Moore-Hodgson-based scheduling, and the consistent advantage of FineServe over Prism* stems from its more efficient use of chunked prefill. Mainly, compared to Prism*, the highest difference in SLO attainment occurred in the case of the request rate scale 2.0 \times and the SLO scale 3.0 \times . Due to the large SLO scale, Prism* tends to batch a large number of requests, and as this batch of requests proceeds with chunked prefill, the likelihood of SLO violations increases. This demonstrates the practical benefit of FineServe’s adaptive batching in meeting latency SLOs under higher request rates.

8 Related Work

Post-Training Quantization (PTQ). PTQ reduces memory footprint and bandwidth by lowering the precision of weights, activations, and the KV cache while keeping a negligible accuracy loss. GPTQ [7] proposes an approximate second-order quantization that maintains accuracy with 3- and 4-bit weights, and SmoothQuant [34] shifts per-channel activation scale into the weights to stabilize INT8 weight-activation quantization. AWQ [14] uses activation statistics to protect salient weights and presents 4-bit weight quantization. FP8 variants exploit FP8 tensor cores to increase arithmetic throughput [32], and QoQ [15] adopts W4A8KV4 precision

to maximize memory savings. FineServe takes the practical adoption of PTQ as a starting point and studies how to serve quantized models at system scale by designing precision-aware KV memory management and scheduling that exploit mixed-precision characteristics.

GPU-based serving system. As GPUs gain more popularity as an accelerator for serving, a wide variety of computer research and systems aim to improve the performance of GPU-based serving systems. Several studies target AI services hosted on private clusters or cloud services [11, 13, 23, 26, 27, 33, 36, 38], while a body of previous work focuses on the better utilization of individual GPUs and memory devices [4, 5, 8, 18, 30].

MuxServe [6] coordinates prefill and decode to improve utilization under latency SLOs, while Splitwise [22] separates the two phases across heterogeneous devices to improve throughput and efficiency. Proteus [1] co-optimizes accuracy scaling and throughput with careful model selection and placement. These systems focus on managing computing resources while memory co-management across co-located models remains to be explored and optimized. FineServe considers each model’s memory footprint and efficiency to steer placement so that contested KV capacity goes to workloads that yield more tokens while guaranteeing SLO.

KV cache memory management. Deployment frameworks based on PagedAttention mechanism, such as vLLM [31] and SGLang [28], maintain a private KV block pool for each model. Hence, models sharing a GPU do not borrow memory from one another. Prism [37] proposes cross-model sharing by using CUDA VMM to preserve contiguous views while mapping physical memory on demand. Frequent map and unmap calls introduce driver overhead, and heterogeneous block layouts can amplify fragmentation [25]. FineServe differs by pre-allocating a shared KV tensor per GPU and dividing it into uniform slabs indexed by KV block size. Compatible models share a slab pool and suballocation stays in user space with tensor views. On top of this, a two-level scheduler places models and sets batching using a memory-efficiency signal so remaining capacity is used where it produces the most tokens while meeting SLOs.

9 Conclusion

We presented FineServe, a mixed-precision LLMs serving framework that addresses memory fragmentation and inefficient GPU sharing. FineServe introduces KV slab, a precision-aware memory manager, and a two-level scheduler that jointly optimize GPU memory and compute allocation. Evaluations with real-world traces show that FineServe achieves up to 2.2 \times higher SLO attainment and 1.8 \times higher token throughput compared to state-of-the-art GPU sharing systems.

References

[1] Sohaib Ahmad, Hui Guan, Brian D Friedman, Thomas Williams, Ramesh K Sitaraman, and Thomas Woo. 2024. Proteus: A high-throughput inference-serving system with accuracy scaling. In *Proceedings of the 29th ACM International Conference on Architectural Support for Programming Languages and Operating Systems, Volume 1*. 318–334.

[2] Anthropic. 2025. Claude. <https://www.anthropic.com/clause>.

[3] Jeff Bonwick et al. 1994. The slab allocator: An object-caching kernel memory allocator. In *USENIX summer*, Vol. 16. Boston, MA, USA.

[4] Seungbeom Choi, Sunho Lee, Yeonjae Kim, Jongse Park, Youngjin Kwon, and Jaehyuk Huh. 2022. Serving Heterogeneous Machine Learning Models on Multi-GPU Servers with Spatio-Temporal Sharing. In *2022 USENIX Annual Technical Conference (USENIX ATC 22)*. USENIX Association, Carlsbad, CA, 199–216. <https://www.usenix.org/conference/atc22/presentation/choi-seungbeom>

[5] Aditya Dhakal, Sameer G Kulkarni, and K. K. Ramakrishnan. 2020. GSILICE: controlled spatial sharing of GPUs for a scalable inference platform. In *Proceedings of the 11th ACM Symposium on Cloud Computing (Virtual Event, USA) (SoCC '20)*. Association for Computing Machinery, New York, NY, USA, 492–506. [doi:10.1145/3419111.3421284](https://doi.org/10.1145/3419111.3421284)

[6] Jiangfei Duan, Runyu Lu, Haojie Duanmu, Xiuhong Li, Xingcheng Zhang, Dahua Lin, Ion Stoica, and Hao Zhang. 2024. MuxServe: flexible spatial-temporal multiplexing for multiple LLM serving. In *arXiv preprint arXiv:2404.02015*.

[7] Elias Frantar, Saleh Ashkboos, Torsten Hoefer, and Dan Alistarh. 2022. Gptq: Accurate post-training quantization for generative pre-trained transformers. *arXiv preprint arXiv:2210.17323* (2022).

[8] Yao Fu, Leyang Xue, Yeqi Huang, Andrei-Octavian Brabete, Dmitrii Ustiugov, Yuvraj Patel, and Luo Mai. 2024. ServerlessLLM: Low-Latency Serverless Inference for Large Language Models. In *18th USENIX Symposium on Operating Systems Design and Implementation (OSDI 24)*. USENIX Association, Santa Clara, CA, 135–153. <https://www.usenix.org/conference/osdi24/presentation/fu>

[9] Amir Gholami, Zhewei Yao, Sehoon Kim, Coleman Hooper, Michael W. Mahoney, and Kurt Keutzer. 2024. AI and Memory Wall. *IEEE Micro* 44, 3 (2024), 33–39. [doi:10.1109/MM.2024.3373763](https://doi.org/10.1109/MM.2024.3373763)

[10] Google. 2025. Gemini. <https://gemini.google.com>.

[11] Arpan Gujarati, Reza Karimi, Safya Alzayat, Wei Hao, Antoine Kauffmann, Ymir Vigfusson, and Jonathan Mace. 2020. Serving DNNs like Clockwork: Performance Predictability from the Bottom Up. In *14th USENIX Symposium on Operating Systems Design and Implementation (OSDI 20)*. USENIX Association, 443–462. <https://www.usenix.org/conference/osdi20/presentation/gujarati>

[12] Woosuk Kwon, Zhuohan Li, Siyuan Zhuang, Ying Sheng, Lianmin Zheng, Cody Hao Yu, Joseph E. Gonzalez, Hao Zhang, and Ion Stoica. 2023. Efficient Memory Management for Large Language Model Serving with PagedAttention. In *Proceedings of the ACM SIGOPS 29th Symposium on Operating Systems Principles*.

[13] Zhuohan Li, Lianmin Zheng, Yinmin Zhong, Vincent Liu, Ying Sheng, Xin Jin, Yanping Huang, Zhifeng Chen, Hao Zhang, Joseph E Gonzalez, et al. 2023. {AlpaServe}: Statistical multiplexing with model parallelism for deep learning serving. In *17th USENIX Symposium on Operating Systems Design and Implementation (OSDI 23)*. 663–679.

[14] Ji Lin, Jiaming Tang, Haotian Tang, Shang Yang, Wei-Ming Chen, Wei-Chen Wang, Guangxuan Xiao, Xingyu Dang, Chuang Gan, and Song Han. 2024. Awq: Activation-aware weight quantization for on-device llm compression and acceleration. *Proceedings of Machine Learning and Systems* 6 (2024), 87–100.

[15] Yujun Lin, Haotian Tang, Shang Yang, Zhekai Zhang, Guangxuan Xiao, Chuang Gan, and Song Han. 2024. Qserve: W4a8kv4 quantization and system co-design for efficient llm serving. *arXiv preprint arXiv:2405.04532* (2024).

[16] Microsoft. 2025. Github Copilot. <https://github.com/features/copilot>.

[17] J Michael Moore. 1968. An n job, one machine sequencing algorithm for minimizing the number of late jobs. *Management science* 15, 1 (1968), 102–109.

[18] Kelvin K. W. Ng, Henri Maxime Demoulin, and Vincent Liu. 2023. Paella: Low-latency Model Serving with Software-defined GPU Scheduling. In *Proceedings of the 29th Symposium on Operating Systems Principles* (Koblenz, Germany) (SOSP '23). Association for Computing Machinery, New York, NY, USA, 595–610. [doi:10.1145/3600006.3613163](https://doi.org/10.1145/3600006.3613163)

[19] NVIDIA. 2025. CUDA Toolkit Documentation: Virtual Memory Management. https://docs.nvidia.com/cuda/cuda-driver-api/group__CUDA__VA.html.

[20] NVIDIA. 2025. Multi-Instance GPU. <https://www.nvidia.com/en-us/technologies/multi-instance-gpu/>.

[21] OpenAI. 2025. ChatGPT. <https://chat.openai.com>.

[22] Pratyush Patel, Esha Choukse, Chaojie Zhang, Aashaka Shah, Íñigo Goiri, Saeed Maleki, and Ricardo Bianchini. 2024. Splitwise: Efficient generative llm inference using phase splitting. In *2024 ACM/IEEE 51st Annual International Symposium on Computer Architecture (ISCA)*. IEEE, 118–132.

[23] Archit Patke, Dhemath Reddy, Saurabh Jha, Haoran Qiu, Christian Pinto, Chandra Narayanaswami, Zbigniew Kalbarczyk, and Ravishankar Iyer. 2024. Queue Management for SLO-Oriented Large Language Model Serving. In *Proceedings of the 2024 ACM Symposium on Cloud Computing (Redmond, WA, USA) (SoCC '24)*. Association for Computing Machinery, New York, NY, USA, 18–35. [doi:10.1145/3698038.3698523](https://doi.org/10.1145/3698038.3698523)

[24] Perplexity AI. 2025. Perplexity. <https://www.perplexity.ai>.

[25] Ramya Prabhu, Ajay Nayak, Jayashree Mohan, Ramachandran Ramjee, and Ashish Panwar. 2025. vattention: Dynamic memory management for serving llms without paggedattention. In *Proceedings of the 30th ACM International Conference on Architectural Support for Programming Languages and Operating Systems, Volume 1*. 1133–1150.

[26] Ruoyu Qin, Zheming Li, Weiran He, Jialei Cui, Feng Ren, Mingxing Zhang, Yongwei Wu, Weimin Zheng, and Xinran Xu. 2025. Mooncake: Trading More Storage for Less Computation — A KVCache-centric Architecture for Serving LLM Chatbot. In *23rd USENIX Conference on File and Storage Technologies (FAST 25)*. USENIX Association, Santa Clara, CA, 155–170. <https://www.usenix.org/conference/fast25/presentation/qin>

[27] Francisco Romero, Qian Li, Neeraja J. Yadwadkar, and Christos Kozyrakis. 2021. INFaaS: Automated Model-less Inference Serving. In *2021 USENIX Annual Technical Conference (USENIX ATC 21)*. USENIX Association, 397–411. <https://www.usenix.org/conference/atc21/presentation/romero>

[28] SGLang. 2025. <https://docs.sglang.ai>.

[29] ShareGPT Team. 2025. ShareGPT. <https://sharegpt.com>.

[30] Haichen Shen, Lequn Chen, Yuchen Jin, Liangyu Zhao, Bingyu Kong, Matthai Philipose, Arvind Krishnamurthy, and Ravi Sundaram. 2019. Nexus: a GPU cluster engine for accelerating DNN-based video analysis. In *Proceedings of the 27th ACM Symposium on Operating Systems Principles* (Huntsville, Ontario, Canada) (SOSP '19). Association for Computing Machinery, New York, NY, USA, 322–337. [doi:10.1145/3341301.3359658](https://doi.org/10.1145/3341301.3359658)

[31] vLLM. 2025. <https://docs.vllm.ai/en/latest/>.

[32] vLLM FP8 Quantization. 2025. <https://docs.vllm.ai/en/v0.5.4/quantization/fp8.html>.

[33] Qizhen Weng, Wencong Xiao, Yinghao Yu, Wei Wang, Cheng Wang, Jian He, Yong Li, Liping Zhang, Wei Lin, and Yu Ding. 2022. MLaaS in the Wild: Workload Analysis and Scheduling in Large-Scale Heterogeneous GPU Clusters. In *19th USENIX Symposium on Networked Systems Design and Implementation (NSDI 22)*. USENIX Association, Renton, WA, 945–960. <https://www.usenix.org/conference/nsdi22/>

presentation/weng

[34] Guangxuan Xiao, Ji Lin, Mickael Seznec, Hao Wu, Julien Demouth, and Song Han. 2023. Smoothquant: Accurate and efficient post-training quantization for large language models. In *International Conference on Machine Learning*. PMLR, 38087–38099.

[35] An Yang, Anfeng Li, Baosong Yang, Beichen Zhang, Binyuan Hui, Bo Zheng, Bowen Yu, Chang Gao, Chengan Huang, Chenxu Lv, et al. 2025. Qwen3 technical report. *arXiv preprint arXiv:2505.09388* (2025).

[36] Gyeong-In Yu, Joo Seong Jeong, Geon-Woo Kim, Soojeong Kim, and Byung-Gon Chun. 2022. Orca: A Distributed Serving System for Transformer-Based Generative Models. In *16th USENIX Symposium on Operating Systems Design and Implementation (OSDI 22)*. USENIX Association, Carlsbad, CA, 521–538. <https://www.usenix.org/conference/osdi22/presentation/yu>

[37] Shan Yu, Jiarong Xing, Yifan Qiao, Mingyuan Ma, Yangmin Li, Yang Wang, Shuo Yang, Zhiqiang Xie, Shiyi Cao, Ke Bao, et al. 2025. Prism: Unleashing GPU Sharing for Cost-Efficient Multi-LLM Serving. *arXiv preprint arXiv:2505.04021* (2025).

[38] Hong Zhang, Yupeng Tang, Anurag Khandelwal, and Ion Stoica. 2023. SHEPHERD: Serving DNNs in the Wild. In *20th USENIX Symposium on Networked Systems Design and Implementation (NSDI 23)*. USENIX Association, Boston, MA, 787–808. <https://www.usenix.org/conference/nsdi23/presentation/zhang-hong>

[39] Yunqi Zhang, David Meisner, Jason Mars, and Lingjia Tang. 2016. Treadmill: Attributing the Source of Tail Latency through Precise Load Testing and Statistical Inference. In *2016 ACM/IEEE 43rd Annual International Symposium on Computer Architecture (ISCA)*. 456–468. doi:10.1109/ISCA.2016.47